Microviscoelasticity of the Apical Cell Surface of Human Umbilical Vein Endothelial Cells (HUVEC) within Confluent Monolayers

Wolfgang Feneberg,* Martin Aepfelbacher,† and Erich Sackmann*
*Technische Universität München, Lehrstuhl für Biophysik E22, Garching, Germany; and †Max von Pettenkofer Institut für Medizinische Mikrobiologie, Universität München, Munich, Germany

ABSTRACT We studied the local viscoelasticity of the apical membrane of human umbilical vein endothelial cells within confluent layers by magnetic tweezers microrheometry. Magnetic beads are coupled to various integrins by coating with fibronectin or invasin. By analyzing the deflection of beads evoked by various force scenarios we demonstrate that the cell envelope behaves as a linear viscoelastic body if forces up to 2 nN are applied for short times (<20 s) but can respond in an adaptive way if stress pulses are applied longer (>30 s). The time-dependent shear relaxation modulus $G(t)$ exhibits three time regimes: a fast response ($t < 0.05$ s) where the relaxation modulus $G(t)$ obeys a power law $G(t) \sim t^{-0.82\pm0.02}$; a plateau-like behavior (at 0.05 s $< t <$ 0.15 s); and a slow flow-like response which is, however, partially reversible. Strain field mapping experiments with colloidal probes show that local forces induce a strain field exhibiting a range of $\zeta = 10 \pm 1$ μm, but which could only be observed if nonmagnetic beads were coupled to the cell surface by invasin. By application of the theory of elasticity of planar bodies we estimated a surface shear modulus of 2.5×10^{-4} N/m. By assuming a thickness of the actin cortex of ~0.5 μm we estimate a Young modulus $\mu \sim 400$ Pa for the apical membrane. The value agrees with a plateau modulus of an entangled or weakly cross-linked actin network of an actin concentration of 100 μM (mesh size 0.2 μm). This result together with our observation of a strong reduction of the shear modulus by the actin destabilizing agent latrunculin A suggests that the shear modulus measured by our technique is determined by the actin cortex. The effect of two ligands inducing actin stress fiber formation and centripetal contraction of cells (associated with the formation of gaps in the confluent cell monolayer) on the viscoelastic responses were studied: histamine and lysophosphatidic acid (LPA). Histamine evoked a dramatic increase of the cell stiffness by >1 order of magnitude within <30 s, which is attributed to a transient rise of the intracellular Ca^{2+} level, since DMSO exerted a similar effect. The stiffening is accompanied by a concomitant rounding of the cells as observed by microinterferometry and relaxes partially in the timescale of 5 min, whereas gaps between cells close after ~30 min. LPA did not exert a remarkable and reproducible effect other than an occasional very weak transient increase of the shear stiffness, which shows that the gap formation activated by LPA is mediated by a different mechanism than that induced by histamine.

INTRODUCTION

The dynamics of numerous chemomechanical processes of cells such as locomotion, endocytosis, or adhesion depends on the viscoelastic properties of the cell envelope: a composite shell consisting of a lipid protein bilayer (the plasma membrane) and the associated actin cortex. The actin cortex of quiescent cells is composed of a partially cross-linked network of the semiflexible filaments of 0.5–1-μm thickness exhibiting a mesh size $\xi = 0.1$ μm (Medalia et al., 2002). The actin filaments are locally attached to the plasma membrane, e.g., through linker molecules mediating the coupling of actin to intracellular domains of cell surface receptors. The coupling proteins comprise members of the ezrin-razin-moesin family in the case of fibroblasts or endothelial cells (compare to Hall, 1998), dystrophin in the case of muscle cells, or talin in the case of cells of *Dictyostelium discoideum* (Merkel et al., 2000; Simson et al., 1998). The actin filaments may also be coupled to the bilayer of the plasma membrane through physisorption of actin coupling proteins exhibiting amphiphatic or positively charged peptide loops, such as talin and vinculin (Tempel et al., 1995; Janmey, 1998) or proteins exhibiting lipid anchors such as hisactophilin.

The plasma membrane forms a continuous fluid film, which exhibits, however, some excess area with respect to the surface area of the actin cortex (Raucher and Sheetz, 1999). This excess area may be organized as shallow protrusion arching toward the extracellular space or as microbuds directed toward the inside, such as coated buds or caveolae. (Interestingly, the storage of excess area in the form of microbuds is commonly observed, if the area of giant vesicles, composed of only one lipid component, is expanded; Häckl et al., 1997.) Moreover, the plasma membrane is an open shell since vesicles continuously detach from and fuse with the membrane during recycling processes. The fusion of vesicles with the plasma membrane plays, e.g., a key role for the growth of axons (Zheng et al., 1991).

The composite cell envelope plays also a key role for the stimulation of cell signaling pathways by external forces. Examples are 1), the control of the blood pressure in blood vessels by stress-dependent stimulation of NO-production through the hydrodynamic shear stress induced by the blood

Submitted November 6, 2003, and accepted for publication January 7, 2004.
Address reprints to Erich Sackmann, E-mail: sackmann@ph.tum.de.

0006-3495/04/08/1338/13 $2.00
doi: 10.1529/biophysj.103.037044

flow (which depends very sensitively on the inner diameters of the blood vessels) and 2), the growth at axon tips or the formation of conical protrusions of macrophages stimulated by external forces of the order of ~100 pN (Vonna et al., 2003).

Various micromechanical techniques for probing local elastic properties at the cell envelope have been developed. These include: 1), the micropipette technique by which forces up to 30 nN can be generated enabling measurements of yield stresses (Evans et al., 1993; Zhelev and Hochmuth, 1995; Merkel et al., 2000); 2), the cell poking technique (Jay et al., 1995) and AFM (Rotsch and Radmacher, 2000; Mathur et al., 2000; Ohashi et al., 2002), which allow local high-resolution measurements of the resistance of the cell surface toward generation of indentations; and 3), the optical tweezers technique, which provides a powerful tool to study the coupling of the plasma membrane to the actin cortex through the pulling of tethers (Raucher and Sheetz, 1999).

In our laboratory we developed the magnetic tweezers technique to measure local viscoelastic parameters (shear moduli, surface shear viscosities, and yield stresses) of cell envelope and cytoplasm, or to estimate active transport forces in cells (Bausch et al., 1998, 1999; Feneberg et al., 2001). In combination with nonmagnetic colloidal probes it is possible to determine the deformation fields induced by local forces to gain insight into the range of the elastic connectivity of selected parts of the cells or to determine elastic moduli of heterogeneously designed materials (Bausch et al., 1998; Boulbitch, 1999). A similar and complementary microrheometry technique is force-free microrheometry, which is based on the analysis of the random walks in terms of the theory of Brownian motions in potentials (Crocker et al., 2000; Tseng et al., 2002).

In this work we continue a previous study (Bausch et al., 2001) on the microviscoelasticity of the apical surface of endothelial cells (HUVEC). We attempted to mimic a more biological situation by studying cells embedded in confluent monolayers which are grown on collagen or microcellulose-coated glass coverslips. We pursued three aims: we first investigated in a systematic manner whether the viscoelastic response is linear (since some evidence for nonlinear behavior was found previously). For this purpose we evaluated the response curves evoked by various force scenarios such as rectangular and triangular force pulses and staircase-like force ramps. We demonstrate that the response is linear for short force pulses of duration $T \leq 20$ s and displacements of <1 μm whereas adaptive (however, partially reversible) deformations are observed after prolonged application of forces of duration $T \leq 30$ s. By application of triangular pulses we estimated the energy dissipated during the shear deformation cycle. We secondly addressed the question whether the viscoelastic response depends on the type of integrin, through which the force probes are coupled to the cell surface by mediating the coupling through fibronectin (FN) (recognizing the integrins $\alpha_5\beta_1$, $\alpha_x\beta_y$, and $\alpha_V\beta_3$) and invasin (INV) (recognizing only integrins with β_1-chains). No appreciable dependence of the viscoelastic response on the type of coupling was observed within the accuracy and reproducibility of our measurements. We thirdly determined the strain field induced by point-like forces by analyzing the induced deflection of nonmagnetic colloidal probes coupled to the cell surface by antibodies to α_2-integrins, FN or INV. Surprisingly, we found only long-range elastic coupling within the cell envelope if colloidal probes were coupled to the cell surface through INV. By analyzing the induced deflection of ~15 force probes we found that the elastic deformation field decreased with a decay length of $l_p = 3$ μm being under the limit of detection at a distance of 10 μm from the force probe. We finally studied the modification of the viscoelastic response by agents, which affect the structure and membrane anchoring of the actin cortex. The effect of the hormone histamine, the growth factor lysophosphatidic acid (LPA), and the actin network destabilizing toxin latrunculin A was evaluated. By real-time measurements of the biochemically induced changes we could follow the response and relaxation of the structural changes with a time resolution of ~10 s.

A remarkable result of these studies is that all agents, studied in the work, induce rapid formation of stress fibers in the basal side of the cell envelope, which are irreversible on the timescale of some hours. In contrast the changes in the apical surface were reversible on the timescale of several minutes and this reversibility correlated well with the closure of the gaps induced by centripetal contraction. Reflection interference contrast microscopy (RICM) enabled us to follow the formation and closure of the gaps between cells.

MATERIALS AND METHODS

Endothelial cells

HUVECs were obtained by cannulating segments of human umbilical cord veins, incubating with α-chymotrypsin (Sigma, Taufkirchen, Germany) for 30 min, and gently irrigating. The irrigant was collected and harvested cells were plated onto collagen-coated (collagen G consisting of 90% collagen I, 10% collagen III; Biochrom, Berlin, Germany) plastic culture flasks. HUVECs were cultured in EGM (Promo Cell, Heidelberg, Germany) containing ECGS/H2 (endothelial cell growth supplement/heparin) and 10% FCS at 5% CO2 and 37°C in a humidified atmosphere. Before the experiment, HUVECs (4×10^4 cells) were plated onto collagen-coated or gelatin-coated cover glasses and grown typically for 4–8 days to form confluent cell monolayers. The cover glasses (lateral dimensions 18×18 mm^2; Menzel Gläser, Braunschweig, Germany) were washed in ethanol and flamed. Before use these cover glasses were coated for 2 h or overnight with 100 mg/ml collagen G (Biochrom) and washed twice with phosphate-buffered saline (PBS, Sigma) to remove nonadsorbed collagen.

Functionalization of the Dynabeads

In all experiments superparamagnetic particles of 4.5-μm diameter (Dynabeads, Dynal, Hamburg, Germany) exhibiting reactive tosyl groups on the surface were used as magnetic tweezers. The beads were bound to specific integrin receptors by coating with two types of ligands: FN and INV.

The beads were coated with these ligands according to the supplier's instructions. Before the experiment 4×10^5 beads were added to the confluent cell monolayer grown on the cover glass and allowed to bind to the cell surfaces for 15–30 min. Finally, the cover glass was mounted in the sample holder of the magnetic bead rheometer and the measurements were started.

Coating of nonmagnetic beads

FN coating

Melamine beads (Polysciences, Warrington, PA) of 2-μm diameter were incubated in a FN solution (50 μg/ml) for 24 h.

Antibody coating

Antibodies against the α_2-chain of integrins were linked to fluorescent beads (Polysciences, Eppelheim, Germany) of 1-μm diameter, which were coated with protein G.

INV coating

INV was covalently bound to 2-μm melamine beads according to a procedure developed in our laboratory (M. Reicheicher and R. Merkel, unpublished data). In all cases successful coating was demonstrated observing the immobilization of the beads on the cell surface. Uncoated beads did not bind to the cell surface but exhibited pronounced Brownian motion above the cell layer.

Measuring chamber and force transducer

The measuring chamber and the magnet have been described in detail previously (Ziemann et al., 1994; Bausch et al., 1998). The magnetic field is generated by a solenoid with a soft iron core exhibiting a nose with a sharp edge. The shape of the iron core was slightly modified compared to the previous studies to enable better adjustment of the microscope's condenser and so to improve the image quality. As shown in Fig. 1, the tip (consisting of a sharp horizontal edge) is shifted upwards with respect to the base by a kink. The nose penetrates the measuring chamber and the distance between cells and the tip of the iron core can be adjusted to a value of $\sim$100 μm. This allows the application of local forces of up to 20 nN. The measuring chamber consists of a copper block, into which an 18×18 mm^2 Teflon frame is fitted serving as a holder for the cover glass with the adherent cells. The measuring chamber contains 100–200 μl of buffer solution, depending on the position of the tip of the iron core. The chamber is covered with a second cover glass to avoid contact with the air. A function generator triggers a custom-built amplifier to activate the magnetic solenoid. The magnet and the measuring chamber are mounted on the stage of an inverted Zeiss Axiovert 10 microscope (Carl Zeiss, Hertfordshire, UK). The calibration of the setup followed earlier methods (Bausch et al., 1998). It was carried out in water-free glycerol by analyzing the trajectories of magnetic beads in terms of an arbitrary fit function $x(t) = a_0 + a_1 t + a_2 t^2 + a\sqrt{t_0 - t}$, where t_0 is the time at which the bead reaches the tip of the magnet. The coefficients a_i were determined by fitting the above equation to the measured trajectories and the bead's velocities at each point were evaluated by differentiating the equation analytically. Using Stokes' law the velocity curves were converted into force curves to obtain the relation between magnetic force and distance to the blade. This calibration was repeated for different coil currents.

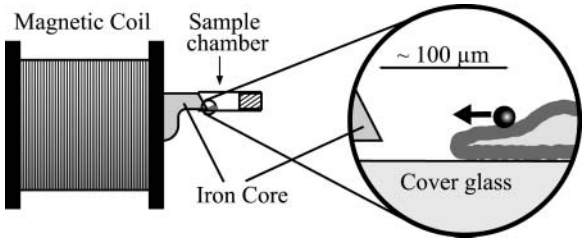

FIGURE 1 Central measuring device of the magnetic bead microrheometer setup. The magnet consists of a coil (1600 turns of 0.7-mm copper wire) and a soft iron core, which penetrates the sample chamber. Note the specific shape of the core close to the coil. This part was slightly modified compared to earlier setups, to enable application of high resolution phase contrast objectives.

For the observation of the cells and the magnetic beads, phase contrast images are taken with a Zeiss Plan-Neofluar objective (40× PH2) and a charge-coupled device camera (C 4880-80 Hamamatsu, Herrsching, Germany) and stored on a PC. The position of the magnetic particles was tracked by the real-time image processing software ''OpenBox'' written in our laboratory (Schilling, 2003). The fastest time resolution achieved with this technique was 8 ms; in most cases the resolution was between 12 and 18 ms, depending on the image size.

Physical basis of microrheometric technique

Our microrheometric technique is based on the analysis of the deflection of magnetic beads (coupled to the extracellular surface of the cell envelope) induced by a sequence of rectangular or triangular force pulses. Although we deal with deformations evoked by local (point-)forces, the well-established concepts of viscoelasticity of bulk bodies can be applied (Bausch et al., 1998; Crocker et al., 2000). In the linear range of elongation the tangential bead deflection $u(t)$, induced by a time-depended force $F(t)$, is proportional to the time derivative of the force, but the proportionality constant is time-dependent and exhibits a memory. Therefore the deflection (measured in units of length) is related to the force by

$$u(t) = \int_{-\infty}^{t} j(t - t') \frac{dF(t')}{dt'} dt'. \quad (1)$$

The value $j(t)$ is the effective, two-dimensional creep compliance (in units of m/N) of the cell envelope. According to a general principle of elasticity—often called St. Vernants principle—the deformation of the surface at large distances from the site of contact does not depend on the shape and size of the local contact between the surface and the bead. We can thus assume the force to be applied to a point on the surface of a large plate (compare to Love, 1944). If the creep response curve $u(t)$ saturates, or if a linear flow regime can be subtracted from the response curve, the stationary value of the effective creep compliance $j_e = j(\infty)$ can be expressed in terms of an effective, two-dimensional shear modulus $\mu^* = j_e^{-1}$. To determine the true two-dimensional shear modulus of the shell one has to determine the strain field. This is achieved in this work by strain field mapping. From the surface shear modulus the bulk modulus μ of the shell can be determined if its thickness d is known according to $\mu^* = \mu/d$.

Strictly speaking, the situation is more complex, since the shear deformation of the cortex may not be homogenous in the out-of-plane direction. As indicated in Fig. 2, the actin cortex is coupled to the intracellular cytoskeleton (e.g., to microtubuli or intermediate filaments). This coupling can formally be accounted for by springs, whose spring constants can be determined, if the strain field in the tangential direction can be measured (compare to Bausch et al., 1998; Boulbitch, 1999; Schmidt et al., 1996). In our case the coupling must be very weak since we do not see any induced motion of intracellular compartments in the short time regime of the deformation. This suggests that we deal with a two-dimensional deformation of the composite cell envelope. This approach is adopted below to determine absolute values of the surface shear modulus and the bulk shear modulus of the actin cortex.

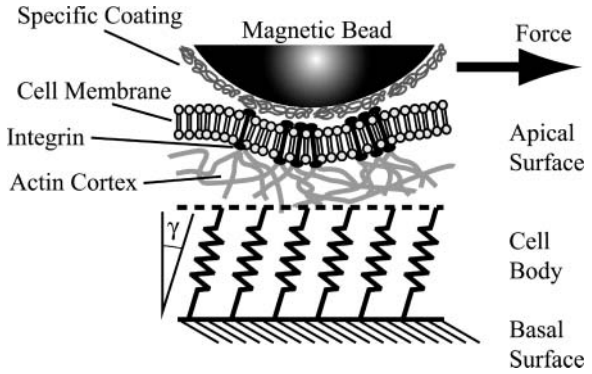

FIGURE 2 Model of the cell envelope as a composite soft shell composed of the lipid-protein bilayer and the associated actin cortex (assumed to form a partially cross-linked network of the semiflexible actin filaments). The force probe is coupled to the actin cortex through integrins. The apical shell of the cell may be coupled to the lower (basal) cell envelope adhering to the substrate (similar to Bausch et al., 1998). The coupling (represented here by springs) can be mediated by the microtubuli and the intermediate filaments of the cytoskeleton.

The formal analysis of the viscoelastic response and relaxation functions evoked by different force scenarios is based on the following considerations:

1. For a stepwise force $F(t)$ switched on at time $t = t_0$ the force may be expressed by a Heavyside function $\Theta(t-t_0)$ (with $\Theta(t < t_0) = 0$ and $\Theta(t > t_0) = 1$) according to $F(t) = F_0\,\Theta(t-t_0)$. The deflection $u(t)$ becomes

$$u(t) = \int_{-\infty}^{t} j(t-t')F_0\delta(t-t_0)\mathrm{d}t' = j(t-t_0)F_0, \qquad (2)$$

where $\delta(t-t_0)$ is the Kronneger δ-function or first derivative of the Heavyside function. Eq. 2 expresses the fact that the deflection at time t depends on the position of the force probe at time t_0.
2. In the linear range of displacement Boltzmann's superposition principle holds. For successive step-changes the applied force can be described as a sum of successive Heavyside functions $F(t) = \sum_1^n \Delta F_i \times \Theta(t - t_i)$, with the step amplitude ΔF_i smaller or larger than zero. The integral becomes thus a sum over all force changes and the deflection is $u(t) = \sum_1^n \Delta F_i \times j(t - t_i)$.
3. The relaxation, also called creep recovery, after the cessation of a force pulse of constant amplitude depends on the degree of shear deformation reached during the onset of the force. It can easily be determined by the application of the principle of linear superposition and by making use of the fact that switching off the force corresponds to the application of a second force step of negative amplitude $-F_0$. The relaxation function for a rectangular force pulse starting at time $t = 0$ and ending at $t = T$ is thus

$$u(t) = F_0\{j(t) - j(t-T)\}. \qquad (3)$$

We will use this relation below to test the reversibility of the viscoelastic response.

RESULTS

Test of linearity of viscoelastic response

Fig. 3 shows a test of the linearity and reproducibility of the viscoelastic response. The deflections of the same bead induced by increasing force pulses normalized with respect to the acting force are plotted. The normalized deflections agree within 10%. Fig. 4 *A* shows the response and the relaxation functions for various pulse lengths (2.5 s $\leq t \leq$ 20s). It is seen that for pulse lengths $T \leq 20$ s the response curves agree well and relax completely. As an example the response to a very long pulse lasting 150 s is shown in Fig. 4 *B*. In contrast to the former behavior, the response for $T >$ 30 s shows an additional increase of the flow velocity at $t >$ 20 s. It is seen that the flow is suddenly accelerated after 30 s. Interestingly, the flow stops suddenly after 120 s.

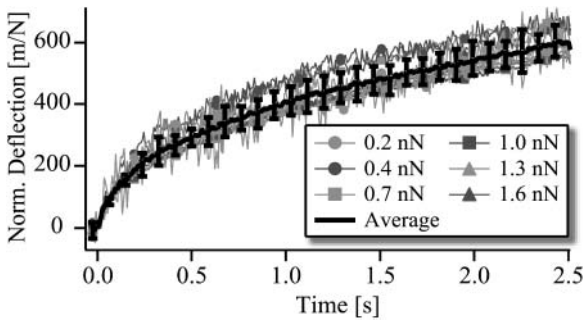

FIGURE 3 Test of linearity of response by forces between 0.2 nN and 1.6 nN. The response curves are normalized with respect to the acting force amplitude and are thus measures of the surface compliance. All curves were determined by a sequence of constant force pulses acting on the same bead whereas the force amplitude increased between two adjacent pulses.

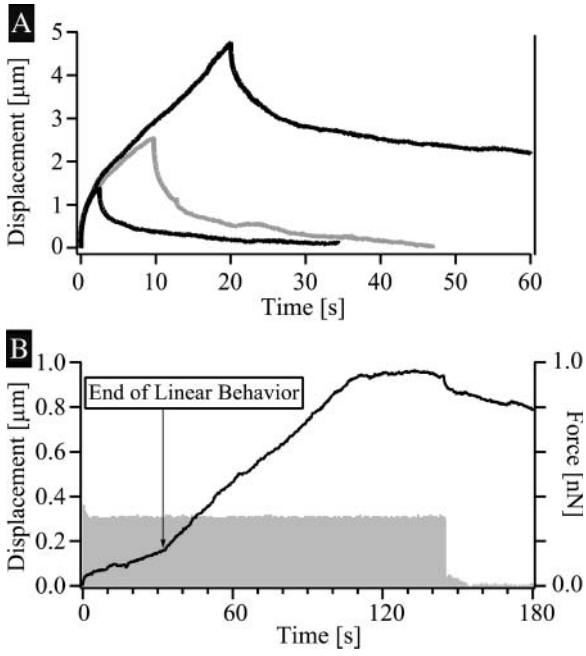

FIGURE 4 Responses of a bead to pulses of different lengths. (*A*) Examples of creep responses induced by short force pulses ($T < 20$ s). Note that all curves are reversible although the response and recovery curves seem to differ in shape (compare to Fig. 7). (*B*) Nonlinear displacement of a bead caused by a long force pulse (145 s). Note the sudden increase of the slope at 30 s and the saturation of the deflection at 110 s.

Similar behavior was found several times, but we did not find a systematic response time of the nonlinear process.

Interpretation of response by a Three-Voigt-Body (TVB) equivalent model

To compare viscoelastic response curves obtained by different micromechanical techniques and to relate these to microscopic dynamic processes it is convenient and helpful to represent the compliance by mechanical equivalent circuits. According to the general principle of linear superposition the compliance can be represented by a sum of retardation functions

$$J(t) = \sum_i J_i(1 - \exp[-t/\tau_i]) \quad (4)$$

characterized by amplitudes J_i and retardation times τ_i. Each term can be modeled by a so-called Voigt-body consisting of a spring (spring constant k_i) and a dashpot (viscosity η_i) in parallel. A rigorous analysis in terms of the retardation functions would require us to consider a whole spectrum of retardation processes. However, despite the fact that we capture a time regime comprising four orders of magnitude with our technique, it is possible to reproduce the response curves within the experimental error by a model consisting of only three Voigt-bodies (compare to Fig. 5 *A*), referred to in the following as TVB-model. In Fig. 5 *B*, the compliances J_i obtained by analyzing response curves of 16 beads on different cells are plotted as functions of the corresponding retardation times. The average retardation times of the three elements differ roughly by an order of magnitude and the variances are smaller than the average distance. The slowest retardation process closely resembles pure viscous flow corresponding to a surface viscosity $\eta \sim 100$ Pa s m. It is seen that each of the three values of J_i vary by an order of magnitude. This corresponds to the variance of the surface elasticity of the cell envelope.

The relaxation modulus *G*(*t*)

The relaxation modulus measured normally by oscillatory experiments can be obtained from the compliance by the convolution method summarized in Appendix A. An example is shown in Fig. 6. A clearly expressed plateau modulus between 0.05 s (20 Hz) and 0.2 s (5 Hz) is found, but the transition into the flow regime starts only at $t > 5$ s. The short time regime $t < 0.05$ s obeys a power law $G(t) \sim t^{-0.8}$. It is interesting to compare these results with the analysis of the creep compliance function $J(t)$ in terms of the TVB-model. Comparison of Fig. 5 *B* and Fig. 6 suggests that the shortest retardation process corresponds to the high frequency regime of $G(t)$, whereas the second Voigt-body characterizes the elasticity within the broad plateau regime and the third Voigt-body characterizes the flow regime (at $t > 5$ s).

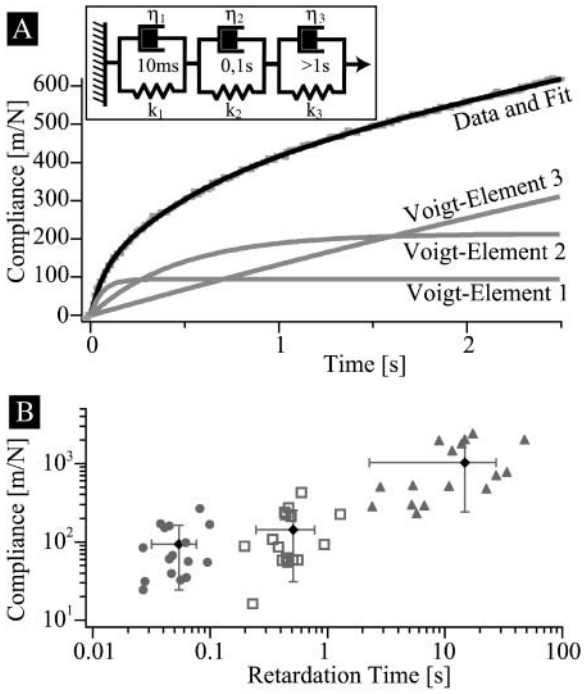

FIGURE 5 (*A*) Analysis of viscoelastic response curves in terms of superposition of three Voigt-bodies in series (called TVB-model in the text). (*B*) Plot of the measured compliances J_i as a function of the retardation times τ_i. The vertical and horizontal bars indicate the variance of 15 measurements. Note that the width of the variance is smaller than the distances of the average relaxation times.

Asymmetry of response and relaxation function

Closer comparison of the response to a magnetic force and the relaxation of the bead after cessation of the force show that the two functions are not symmetric. The creep recovery often appears to exhibit long tails (compare to. Fig. 4 *A*, short force pulse; see also Bausch et al., 2001). To check whether this is due to some nonlinear behavior of the viscoelastic response we calculated the creep recovery from the retardation function by application of the linear superposition

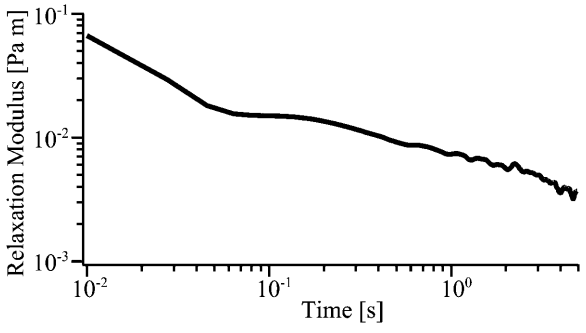

FIGURE 6 Example of relaxation modulus $G(t)$ reconstructed from the creep compliance following the convolution procedure described in Appendix A.

theory. According to the linear theory (Ferry, 1980) the total viscoelastic response can be divided into a deflection evoked by a step-like force of amplitude F_0 applied at $t = 0$ and by a negative step-like force of amplitude $-F_0$ applied at $t = T$. The decay curve is then expected to be expressed by Eq. 3: $u(t) = F_0(j(t)-j(t-T))$. To test the validity of this equation, the decay curve $u(t > T)$ was calculated numerically from an arbitrarily chosen creep compliance evoked by a rectangular force pulse of length T. This curve was then compared with an experimental decay curve of a response of the same pulse length. As demonstrated in Fig. 7 excellent agreement is achieved between the calculated and measured creep recovery demonstrating again the linearity of the response for short pulses. An important conclusion suggested by Eq. 3 is that the response and relaxation functions are only symmetric if the response saturates within the time T of the pulse length (compare to Bausch et al., 1998), whereas long tails appear if the creep compliance does not reach a constant value within the time T.

Triangular force pulses and energy dissipation

As a further test of the linearity of the viscoelastic response we analyzed the response function evoked by symmetric triangular force pulses. This force scenario allows simultaneous measurements of the deflection-versus-force diagrams. Fig. 8 shows a typical response curve together with a simulation of the response based on the principle of linear superposition. This principle predicts that the deflection $u(t)$ is related to the time derivative of the force dF/dt as

$$u(t) = \int_0^t j(t-t')\frac{dF(t')}{dt'}dt', \qquad (5)$$

with $dF/dt = +F_0$ for $0 < t < T/2$ and $dF/dt = -F_0$ for $T/2 < t < T$. To test the validity of this approach we measured the compliance $j(t)$ evoked by a rectangular force pulse of the same amplitude. This experimental curve $j(t)$ was then inserted into Eq. 5 to calculate the response induced by the ascending and descending branch of the triangular force pulse. If one assumes that the force pulse is perfectly triangular, the measured and calculated curves agree qualitatively; that is, $u(t)$ still increases whereas the force decreases, but they differ quantitatively by 10%. Excellent agreement is achieved (compare to *black line* in Fig. 8), however, if we take into account that for small coil currents the superparamagnetic beads are not completely saturated and that the force therefore starts to increase quadratically with the current (Ziemann et al., 1994). In separate experiments it was shown that this quadratic regime holds for currents <250 mA as indicated by the arrow in Fig. 8, whereas the magnetic force increases linearly for larger currents when the beads are completely magnetized.

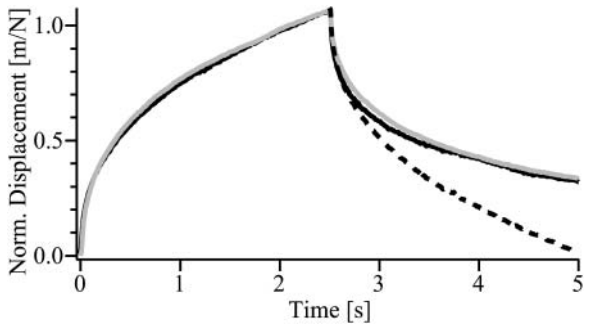

FIGURE 7 Shaded curve is creep response and creep recovery curve induced by a rectangular force pulse of $T = 2.5$ s duration. The black line is calculated from a measured creep compliance by application of the linear response principle Eq. 3. The dotted line is the negative creep compliance $-J(t-T)$ to indicate the difference between the recovery curve and the displacement curve.

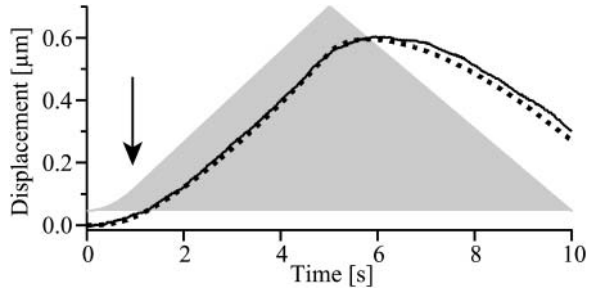

FIGURE 8 Comparison of measured (*solid line*) and calculated (*dotted line*) bead deflection evoked by a triangular force pulse (*light shaded area*). The calculation was carried out using an experimental response to a square pulse and determining the numeric solution of the convolution Eq. 5. Note that the triangular force experienced by the bead starts with a parabolic initial phase (its end is indicated by an *arrow*) due to the fact that the magnetic bead is not fully magnetized at small coil currents.

An interesting benefit of symmetric triangular pulses is that they enable us to measure deflection-force diagrams. An example is presented in Fig. 9. According to the well-known principles of hysteresis (Ferry, 1980) the area between the displacements obtained for increasing and decreasing forces is a measure for the energy dissipated during one cycle of the oscillatory force. Fig. 9 yields an energy dissipation of

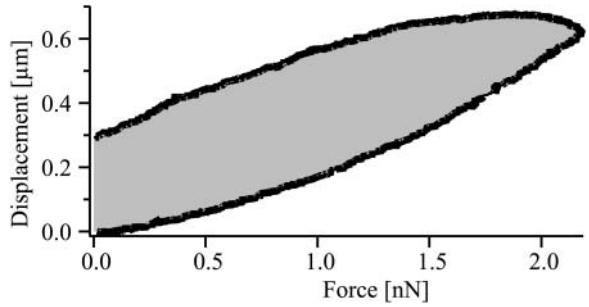

FIGURE 9 Displacement versus stress diagrams determined from the ascending and descending branch of the response induced by a triangular force pulse.

$0.70 \cdot 10^{-15}$ Nm. Note that this is a lower limit since, as described above, the relaxation is delayed.

Strain field mapping

The viscoelastic parameters obtained by analyzing the viscoelastic response curves in terms of equivalent circuits yield relative measures of the shear modulus and the surface viscosities of the cell envelope. To determine absolute elastic moduli of the cell envelope the range of the deformation field generated by point forces must be determined. For this purpose nonmagnetic colloidal probes were coupled to specific integrins through FN (recognizing $\alpha_V\beta_3$), antibodies against α_2-integrins, or INV (recognizing integrins with β_1-chains). A striking result of these experiments is that only nonmagnetic beads bearing INV showed observable deflections. As an example Fig. 10 shows a phase contrast micrograph of HUVECs with two attached magnetic beads (*M1* and *M2*), and 11 nonmagnetic probes (*L1*...*L11*) coupled to the cell surface through INV. The arrows indicate (10 times enlarged) the amplitude and direction of deflection. A detailed analysis shows that only the nonmagnetic beads L3, L5, L8, and L9 exhibit induced motion, whereas the other beads are not deflected appreciably, although some of them are in the same range of distance to the magnetic beads. Closer inspection of Fig. 10 and other cases of induced deflections show that, although the deformation field clearly decays with the distance from the point source, it does not correspond to a homogenous plate strongly suggesting some anisotropic structure of the actin cytoskeleton. To gain quantitative insight into the decay of the deformation field we analyzed the radial distance dependence of the deflection of 23 nonmagnetic beads and the result is shown in Fig. 11. The deflection decays clearly with the radial distance from the center of the force. By approximating the data points by an exponential curve one finds a decay length of $l_p = 3\ \mu$m. The fit assumes the value $u(r) = 1$ at a distance of $r = 1.8\ \mu$m which is slightly smaller than the bead radius and can thus be considered as the radius of the contact area. Note that at a distance of 11 μm the expected deflection is below the limit of spatial resolution.

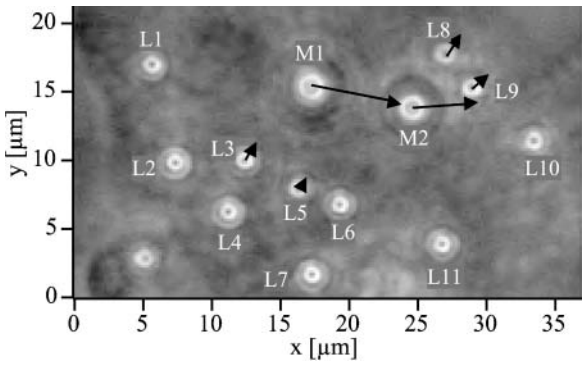

FIGURE 10 Phase contrast micrograph of endothelial cells with magnetic beads (*M1*, *M2*) and nonmagnetic probe beads. The white arrows indicate the deflections of the beads at 10-fold enlargement.

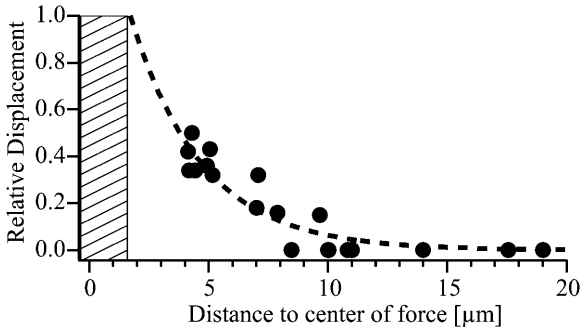

FIGURE 11 Plot of relative deflections of nonmagnetic probes coupled to endothelial cell surface through INV as a function of the radial distance form the point force. The data were obtained by analyzing 18 beads on nine cells. The dashed line is an exponential fit to the data points. The fit assumes the value 1 at a distance of 1.8 μm from the origin, which is assumed as the radius of the adhesion area of the magnetic bead.

Effect of histamine

The effect of the hormone histamine (10 μM) on the viscoelasticity of the cell envelope is studied in Fig. 12 by repeated recording of the bead deflection evoked by a sequence of pulses of $T = 2.5$ s duration and 2-nN force amplitude. The interruption of image recording during the addition of histamine to the sample chamber until the first possible response experiment is at most 30 s. During this time the stiffening of the cell envelope is so strong that the response amplitude evoked by a 2-nN force is barely observable. Fig. 12 *A* also shows that the effect of histamine is partially reversible with a recovery time of ~180 s. The analysis of the creep responses in terms of the TVB-model shows that the slow flow-like component is still suppressed after 180 s, whereas both elastic responses recover nearly completely (compare to Fig. 12 *B*). In separate experiments (not shown here) we observed the contact area and the shape of the apical membrane close to the boundaries between adjacent cells by reflection interference contrast microscopy (RICM). It was found that the apical membrane of all cells are retracted ~50 s after addition of histamine, strongly suggesting that the stiffening of the actin cortex is accompanied by lateral contraction of the cell envelope. The formation of gaps between cells occurs in the same timescale but not between all cells.

Effect of latrunculin A

To explore the role of the actin cortex on the viscoelasticity of the cell envelope we studied the effect of latrunculin A. This toxin of sponges from the Red Sea strongly binds to actin monomers, thus preventing the polymerization of new

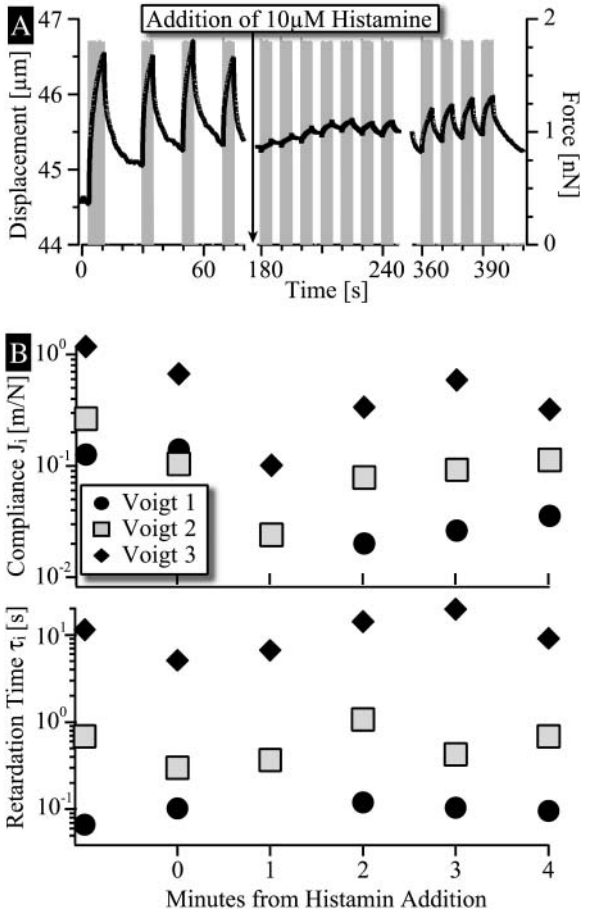

FIGURE 12 Effect of histamine on the viscoelastic response of the endothelial cell envelope. (*A*) Deflection of magnetic bead induced by a sequence of force pulses of $T = 2.5$ s and $F = 1.8$ nN. 10 μM of histamine was added into the sample chamber at the time indicated by the arrow. (*Note that only partial recovery is observed after 4 min (B)*) Analysis of the stiffening caused by histamine in terms of the TVB-model: time evolution of the compliances J_i.

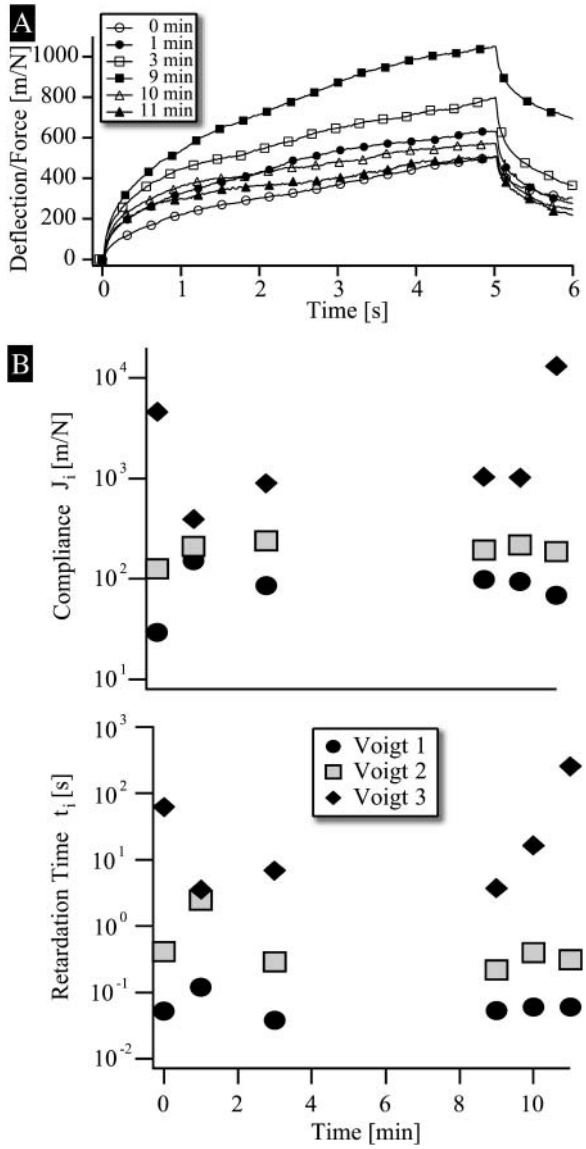

FIGURE 13 Demonstration of reversible softening of apical endothelium envelope by latrunculin A, a toxin from sponges which binds strongly to actin monomers and thus impedes the formation of new actin filaments by sequestering dissociated actin monomers. (*A*) Time evolution of the bead deflection after addition of 0.01 μM latrunculin A to the sample chamber. The deflection increases by approximately a factor of 5 after the addition of the agent. The deflection decreases nearly to the original value after 11 min although the shape of the retardation function differs from the original curve due to some irreversibility of J_3. (*B*) Analysis of the deflections in terms of the TVB-model. Note that J_3 relaxes only partially after 11 min.

actin filaments while sequestering dissociated G-actin. A series of response curves recorded at different times after the addition of a low concentration of latrunculin A (0.01 μM), which is added at time $t = 0$, is shown in Fig. 13 *A*. Fig. 13 *B* shows the analysis of the effect of latrunculin A in terms of the TVB-model. Within 2 min the impedance J_1 increases by a factor of 2, whereas J_2 remains nearly constant. In contrast the compliance of the slow flow-like component decreases by a factor of 10 during the first minute. Similar to the behavior found for histamine the effect of latrunculin A is only partially reversible. Thus, judged from Fig. 13 *B* the compliance J_1 does not relax completely after 11 min.

Effect of other agents: DMSO and nocodazole

A conventional way to apply biochemicals, which do not permeate the cell membrane such as latrunculin A, is the use of DMSO. As a control experiment we checked the time evolution of the compliance of the cell envelope induced by application of 1% DMSO (results not shown), which is 10 times larger than the concentration used in our experiments. A stiffening of the cell envelope is observed, which relaxes after 3 min. The effect of the microtubuli-decomposing agent nocodazole was tested by adding 10 μM dissolved in 0.1% DMSO. No appreciable effect on the viscoelastic response was observed despite the application of the drug with DMSO solution.

DISCUSSION

The present work provided additional evidence that the magnetic bead microrheometry is a useful technique to characterize the mechanical behavior of the cell envelope in terms of local viscoelastic moduli and surface frictional coefficients by analyzing the response and decay curves for different force scenarios. We show that the cell envelope exhibits linear viscoelastic behavior with respect to short time deformations (pulse durations $T_f \leq 20$ s) and that the deflections are completely reversible. At longer times of force application, however, the endothelial cells can respond in an adaptive way by in-plane flow of the force probe over several micrometers. In this case the nucleus is also displaced. In some cases we observe that after several hundred seconds the bead motion stops, indicating an active response of the cells.

The magnetic bead microrheometry is a noninvasive technique, but the coupling of the force probe to the cell surface receptors will in general induce a local reorganization of the actin cortex. Thus binding of the magnetic beads to the cell surface can induce the clustering of integrins leading to the recruitment of ring-like assemblies of actin. The formation of such rings by binding of FN-coated beads was previously observed (Bausch et al., 2001, Miyamoto et al., 1995). The recruitment of dense actin assemblies by binding of INV-bearing objects for phagocytosis is well established (Young et al., 1992). On the other hand, the induced actin assemblies with the adsorbed force probes reflect real biological situations of particles (e.g., pathogenic bacteria) adhering to the cell surface.

We did not observe any remarkable effects of local force pulses on the viscoelastic behavior of the endothelial cells even after application of several pulses (up to 20, compare to Fig. 3). This is in contrast to the behavior of stromal cells (fibroblast of connective tissue) for which an increase of the cell stiffness by a factor of 6 was induced by repeated application of forces through magnetic beads (Glogauer et al., 1997).

On the origin of the viscoelastic behavior of cell envelope

In the following we argue that microviscoelastic behavior of the cell envelope is determined by the actin cortex. First evidence comes from the experiment with latrunculin A. As demonstrated in Fig. 13 this toxin leads to a softening of the short time elasticity, but renders the cell envelope more resistant to the slow (flow-like) deformation. Latrunculin A is known to inhibit participation of G-actin in polymerization since it binds strongly to actin monomers competing with the sequestering protein thymosin β which controls prolongation of fast growing ends (Yarmola et al., 2000). The softening effect can thus be understood in terms of the decomposition of the actin cortex by preventing the repolymerization of actin monomers dissociating from the actin filaments. The impediment of the very slow deflection mode is more difficult to explain. One possibility is that the slow motion is associated with the force-induced unbinding and the reformation of new bonds within the actin cortex and between the actin and the plasma membrane. Since this turnover is inhibited by latrunculin A the contribution of such a mechanism to the flow-like behavior of $J(t)$ would be suppressed.

The second evidence, that the viscoelasticity of the cell envelope is mainly determined by the actin cortex, is provided by the analysis of the retardation function $J(t)$ in terms of the series connection of Voigt-bodies revealing three time regimes: 1), a short time response with retardation time $\tau_1 \sim 0.05$ s; 2), a medium time response ($\tau_2 \sim 0.5$ s); and 3), a very slow deflection ($\tau_3 \sim 10$ s). This behavior of $J(t)$ is reflected by the relaxation modulus $G(t)$ which also exhibits three clearly distinguishable time regimes: a short time regime, a plateau regime, and flow-like behavior. In contrast to Fabry et al. (2001), we do not find a universal scaling law over four decades of time. The time dependence of the relaxation modulus of the fast response follows a scaling law $G(t) \sim t^{-0.82\pm0.02}$, which agrees reasonably well with the high-frequency behavior of the relaxation modulus of entangled and cross-linked actin networks and which is known to be determined by the entropic tension of the actin filaments (Tempel et al., 1995).

Some further evidence for our conjecture that the viscoelasticity of the cell envelope is determined by the actin cortex is provided by comparing the shear modulus in the plateau regime with the plateau moduli of in vitro actin networks. To do this we have to determine the Young modulus of the cell envelope. Fortunately this is possible at least approximately in our case due to the measurement of the deformation field. As shown in Fig. 11 the deformation caused by the magnetic force probe decays with the distance from the point force with a decay length of $R_c \sim 3$ μm. In a previous study on the viscoelasticity of fibroblast cells we showed that the decay of the deformation field can be explained in terms of coupling of the apical membrane to the basal one. This was possible since the apical envelope of the thin lobes of spread single cells was studied, and the space between the two membrane surfaces is filled with cross-linked actin. In the present work on confluent cell monolayers, however, the apical envelope was well separated from the surface of the substrate (e.g., by the nuclear region of the cell). Since we did not find evidence for induced deflection of cytoplasmic compartments we assume that we are dealing with the situation of tangential deformation of an infinitely large plate by a local homogenous force acting in the tangential direction along a vertical axis penetrating the shell. The force is assumed to be homogeneous along directions normal to the plate and is expressed in terms of force per unit length. The deformations u and v in the direction parallel and perpendicular to the force direction are given in Appendix B. Unfortunately, the theoretical deformation field consists not

only of a component, which decays with the radial distance logarithmically, but also of a constant component accounting for the variation of the deformation with the polar angle with respect to the force direction. We can overcome this problem, however, by considering the difference of the deflections at two different radial distances from the origin yielding

$$u(r_1) - u(r_2) = \frac{1}{4\pi\mu^{(3\,\mathrm{dim})}} \frac{F}{d} \ln(r_1/r_2), \qquad (6)$$

where d is the thickness of the cortex and $\mu^* = \mu \cdot d$ is the surface shear modulus. Inserting the data from Fig. 11 we obtain a surface shear modulus of $\mu^* = 2.5\ 10^{-4}$ N/m and a bulk modulus of 400 Pa assuming a thickness of the cortex of 0.5 μm.

A different approach to relate the deflection to the local force is to assume that the deflections are small compared to the thickness of the cell envelope. In this case we deal with the situation of a local tangential force applied to the surface of a large body. The deformation field decays hyperbolically with distance. For deflections along the axis of the force direction one obtains (again by assuming for simplicity that the network is incompressible) $u = (1/16\pi\mu)(F/r)$ (compare to Landau and Lifshitz, 1986). The value μ is again the bulk shear modulus, which we can determine by analyzing the decay of the deflection. One obtains $\mu = 20$ Pa, which is one order-of-magnitude smaller than the value obtained with the first approach. Since the measured deflections (0.1–1 μm) are comparable to the thickness of the plate we consider this approximation less reliable. It is interesting to compare the data with the surface shear modulus for erythrocytes: $\mu^{(2\mathrm{dim})} = 6 \cdot 10^{-6}$ Pa m (Evans and Skalak, 1980). The thickness of the spectrin actin network of erythrocytes is $\sim d \sim 0.6$ μm. This would correspond to a bulk shear modulus of 10 Pa.

We compare now the shear modulus obtained by the above analyses with values of the plateau modulus G' of in vitro actin networks cross-linked by α-actinin (Tempel et al., 1995). For an actin concentration of $c_A = 10$ μM the plateau modulus in the entangled and partially cross-linked state (average distance between cross-linkers smaller or equal to mesh size) is $G' \approx 0.1$ Pa and in the completely cross-linked state $G' \approx 10$ Pa. The concentration of polymerized actin in mammalian cells is $c_A \sim 50$ μM (Pollard and Earnshaw, 2002). If we assume that all actin is confined to the cortex of thickness $\delta \sim 1$ μm of a cell of radius $R \sim 20$ μm, the effective actin concentration is $c_A^* = 350\,\mu$M. For a strongly cross-linked network the plateau modulus is related to the actin concentration by the scaling law $G'(c_A) \sim c_A^{5/2}$ (MacKintosh, 1998). For partially crosslinked or entangled networks the scaling law $G'(c_A) \sim c_A^{7/2}$ holds (Hinner et al., 1998). One therefore would expect a value of the Young modulus of the cell envelope of $G' = 5\ 10^4$ Pa if the actin network was strongly cross-linked and of $G' \sim 500$ Pa, if the network was weakly cross-linked, since weak cross-linking or entangling does not increase the shear elasticity remarkably (compare to Tempel et al., 1996) The latter value agrees well with the shear modulus $\mu \sim 400$ Pa of the cell envelope obtained by the above analysis.

In summary, the above analysis leads to the conclusion that the actin cortex of the apical envelope is only weakly cross-linked and that the surface shear elastic modulus is only by approximately a factor of 50 larger than that of erythrocytes.

It should be emphasized that (as noted above) binding of the nonmagnetic beads to the cell surface through INV may disturb the local organization of actin. Some evidence comes from the finding that the observed deflections deviate from the direction predicted by elastic models of isotropic bodies and also from the large scattering of the data in Fig. 11. However, the well-defined decay of the elastic deformation field provides strong evidence that the perturbations induced by binding of the force probes is a local effect and that the strain field measured in Fig. 11 reflects the behavior of the quiescent state of the cell.

On the origin of membrane stiffening by actin cross-linking

We studied the effect of two extracellular activators of signaling pathways known to cause a reorganization of the actin-based cytoskeleton and are thus expected to modify the viscoelasticity of the cell envelope: histamine and LPA. Both agents are known to lead to the formation of actin/myosin bundles and stress fibers resulting in the centripetal contraction of the cells and the formation of gaps between cells of the confluent endothelial cell layers (Garcia and Schaphorst, 1995; Moy et al., 1996; Andriopoulou et al., 1999; Aepfelbacher and Essler, 2001, Siess et al., 1999). Similar to thrombin (Bausch et al., 2001) histamine induces a rapid but transient stiffening of the apical cell envelope. In contrast LPA reduces the shear elasticity at most by a few percent for a short time (compare to Bausch et al., 2001). However, it also induces the formation of stress fibers and the opening of gaps between the cells. This strongly suggests that the stiffening and unbinding of cell-cell contacts are different events. Histamine induces the rapid weakening of cadherin-mediated cell-cell contacts by decoupling of cadherin from the actin cortex and the intermediate filaments (e.g., vimetins) fraction of the cytoskeleton (Shasby et al., 2002). LPA acts in a more indirect way through activation of Rho-GTPases (Moolenar et al., 1997).

The following consideration suggests that the histamine-induced stiffening is due to cross-linking of the actin cortex. According to Fig. 12, 10-μM histamine (a 10-times-smaller concentration than in Andriopoulou et al., 1999) reduces the compliance by two orders of magnitude, suggesting that the shear modulus increases from $G \sim 500$ Pa to $G^* \sim 5$ kPa.

This corresponds well with the increase of the plateau modulus of an entangled actin network by complete cross-linking with α-actinin (*complete* means that the density of active cross-links is equal or higher than to the density of the sites of steric interaction of the actin filaments (compare to Tempel et al., 1995).

The next question is which cell signaling process is activated by histamine. Several possibilities are suggested in the literature. One likely possibility is that histamine acts through the Rho-type GTPase Cdc42, the activation of which leads to the nucleation of actin polymerization by WASp proteins and furthermore activates actin growth, which initiates polymerization by uncapping of gelsolin (Hall, 1998). Evidence for this interpretation is provided by the strong increase of the fraction of polymerized actin resulting in the formation of stress fibers (Andriopoulou et al., 1999). Moreover, the effect caused by Cdc42 is known to be very fast (Hall, 1998), such as the histamine-activated stiffening effect.

A second reason for the rapid stiffening could be the rapid formation of actin/myosin bundles by phosphorylation of the myosin light chains (MLC). This process can be mediated by activation of MLC kinases or inhibition of MLC phosphatases through Ca^{2+}/Calmodulin or Rho/Rho-kinase, respectively. In the case of thrombin, the Ca^{2+}-mediated pathway is triggered by the increase of intracellular Ca^{2+} (within 60 s according to Garcia and Schaphorst, 1995), which is accompanied by an equally fast decrease of MLC-phosphatase resulting in MLC-phosphorylation (Essler et al., 1998, 1999). The Ca^{2+}-mediated pathway is most likely also responsible at least partially for the histamine effect. This could explain the difference between histamine and LPA since the latter agent does not increase intracellular Ca^{2+}-level (Amerongen et al., 2000). It is also suggested by our observation that Ca^{2+}-influx mediated by DMSO leads to a similar strong stiffening effect (Feneberg, 2003).

At the present state of the experiments we cannot distinguish between the two mechanisms mentioned above. Judged from in vitro experiments on the viscoelasticity of actin/myosin networks in our laboratory the formation of actin-myosin bundles does not lead to strong stiffening at excess ATP but only after ATP depletion. A Cdc42-mediated increase of the polymerized actin fraction and cross-linking by Arp-linkers is thus the more likely pathway.

RICM shows that the retraction of the apical cell membranes observed by microrheometry is an important consequence of the stiffening of the actin cortex as the generation of a strong cortical tension. This leads to a strong centripetal contraction force on the adhering cells. This tension, together with the weakening of the cell-cell adhesion forces, is the driving force responsible for the gap formation.

It should also be noted that long time observations of the effects of all stimulating agents over 1 h is often impeded by cell damage. This is indicated by the appearance of pronounced membrane bending fluctuations (flickering). This effect may be attributed to the decoupling of the actin cortex from the plasma membrane.

CONCLUDING REMARKS

We demonstrate that microrheometry with colloidal force probes is a useful tool to quantitatively characterize the local mechanical properties of the cell envelope and changes induced by intracellular signaling in terms of local viscoelastic parameters. By measuring the deformation field induced by local forces it is possible to determine local shear elastic moduli of the cell envelope. In the quiescent state of the cells the values measured with our technique agree rather well with the shear modulus of slightly cross-linked or entangled actin networks exhibiting mesh sizes of $\xi \sim 0.1$ μm. By application of different force scenarios it was possible to show that the endothelial cell envelope behaves as an ideal linear viscoelastic body toward nanoNewton force pulses of up to 30-s duration, whereas the cells respond in an adaptive way if the forces are applied longer. The microrheometry enables new insight into the changes of the mechanical properties of the cell envelope by cell-stimulating or cell-damaging agents. One example is the observation of distinct differences between the mechanisms of LPA- and histamine-induced gap formation in confluent endothelial cell layers. Histamine, similar to thrombin, induces gap formation by simultaneous generation of a strong cortical tension and weakening of cadherin-mediated cell-cell contacts, whereas LPA appears to mediate the gap formation by a more subtle mechanism (without Ca^{2+} influx) mediated by Rho-GTPases. This is consistent with the observation that gaps induced by histamine or thrombin are larger than those generated by LPA stimulation.

The present work is to some extent still a feasibility study, which shows that local viscoelastic moduli can be measured by analysis of well-defined modes of deformation and measurements of the range of deformation fields. The softness of the apical endothelial membrane observed by us seems to conflict with measurements based on AFM. However, in these experiments the thin cell lobes at the rim of the cell are normally studied which exhibit much higher stiffnesses as follows from the fact that our forces are too weak to evoke observable deflections in this case.

To relate viscoelastic moduli to the structure of the cytoskeleton in a more direct way magnetic bead microrheometry can be easily combined with other microscopic techniques such as microfluorescence and microinterferometry. Further insight can be gained by simultaneous measurements of the viscoelastic moduli of the cell envelope and the cytoplasm (Bausch et al., 1999). Another, technically more elaborate way to characterize local mechanical properties of cells would be to measure local forces by feedback systems.

APPENDIX A: NUMERICAL SOLUTION OF THE CONVOLUTION INTEGRAL

The viscoelasticity of bulk bodies can be characterized by two time-dependent moduli:

1. The relaxation modulus $G(t)$, which is determined by measuring the elastic shear stress $\sigma(t)$ induced by an enforced deformation $\gamma(t)$ according to $\sigma(t) = \int_{-\infty}^{t} G(t-t')(d\gamma(t')/\mathrm{d}t')\mathrm{d}t'$.
2. The retardation modulus $J(t)$ (creep compliance), which is determined by measuring the (shear) strain (defined as the shear angle) of the body evoked by a time-dependent applied (shear) stress $\sigma(t)$ according to $\gamma(t) = \int_{-\infty}^{t} J(t-t')(d\sigma(t')/\mathrm{d}t')\mathrm{d}t'$.

Due to the fact that the deformation (or stress) induced by a transient stress (or strain) depends on the prehistory the two moduli are interrelated by a convolution

$$\int_0^t J(t-t')G(t')\mathrm{d}t' = t. \tag{A1}$$

The relationship Eq. A1 enables us to reconstruct the relaxation modulus from the measured retardation modulus numerically as follows:

The integral in Eq. A1 is replaced by a sum of integrals $t = \sum_{i=0}^{n-1} \int_{t_i}^{t_{i+1}} J(t-t')G(t')\mathrm{d}t'$, where $t_0 = 0$ and $t_n = t$. If $G(t)$ is now assumed to be constant in each integral and equal to $G(t_{i+1/2})$, it is possible to drag this term in front of the integral. By solving the remaining integral over $J(t-t')$ numerically one can calculate $G(t)$. In our analysis we took as time intervals the distance of data points, i.e., Δt is between 8 ms and 18 ms.

APPENDIX B: DEFORMATION FIELD OF A PLANAR ELASTIC BODY

We consider an infinite plate of thickness d, which is deformed by a local force in a tangential direction along a vertical line through the plate. According to a general principle of elasticity (Love, 1944) one can replace the line by a cylindrical cavity, which is bound by a circle with its center at the origin of a coordinate system (x,y,z), where z is the axis of the cylinder (perpendicular to the plate) and x the direction of the force. If we assume the plate to be incompressible, the deformations u and v in the direction parallel and perpendicular to x, respectively, are then given by

$$u = \frac{F}{4\pi\mu d}(\ln r + \cos^2\vartheta)$$

$$v = \frac{F}{4\pi\mu d}(\sin\vartheta\cos\vartheta). \tag{B1}$$

F/d is the force per unit length, r is the radial distance from the origin, ϑ is the polar angle defined with respect to the force direction, and μ is the bulk modulus of the plate. We can define $\mu^* = \mu\, d$ as the surface shear modulus with the dimension [Pa m]. A mathematical difficulty of this solution of the planar problem is that the direction-dependent contribution in Eq. B1 does not decay to zero at infinite distance. However, the solution may be considered to be composed of a near-field of deformation decaying logarithmically with distance and a constant long-range deformation field. One can also see that the nondecaying component vanishes along the direction perpendicular to the force. Despite the mathematical difficulties the above equations can be applied to estimate the shear modulus in our case since we could measure the decay of the deformation field which is determined by the logarithmic term in Eq. B1 alone.

The help of C. Trasak and G. Cheml with the preparation of the endothelial cell layers and of B. Lorz with RICM microscopy is gratefully acknowledged.

The work was supported by the Deutsche Forschungsgemeinschaft (SFB 413) and the Fonds der Chemsichen Industrie.

REFERENCES

Aepfelbacher, M., and M. Essler. 2001. Disturbance of endothelial barrier function by bacterial toxins and atherogenic mediators: a role for Rho/Rho-kinase. *Cellular Microbiol.* 3:649–658.

Amerongen, G. P. v. N., M. A. Vermeer, and V. W. M. van Hinsbergh. 2000. Role of RhoA and Rho-kinase in lysophosphatidic acid-induced endothelial barrier dysfunction. *Arterioscler. Thromb. Vasc. Biol.*, 20: e127–133

Andriopoulou, P., P. Navarro, A. Zanetti, M. G. Lampugnani, and E. Dejana. 1999. Histamine induces tyrosine phosphorylation of endothelial cell-to-cell adherens junctions. *Arterioscler. Thromb. Vasc. Biol.* 19: 2286–2297.

Bausch, A. R., U. Hellerer, M. Essler, M. Aepfelbacher, and E. Sackmann. 2001. Rapid stiffening of integrin receptor actin linkage in endothelial cells stimulated with thrombin. A magnetic bead microrheology study. *Biophys. J.* 80:2649–2657.

Bausch, A. R., W. Möller, and E. Sackmann. 1999. Measurement of local viscoelasticity and forces in living cells by magnetic tweezers. *Biophys. J.* 76:573–579.

Bausch, A. R., F. Ziemann, A. Boulbitch, K. Jacobson, and E. Sackmann. 1998. Local measurements of viscoelastic parameters of adherent cell membranes by magnetic bead microrheometry. *Biophys. J.* 75:2038–2049.

Boulbitch, A. A. 1999. Strain of a biomembrane caused by a local tangential force: application to magnetic tweezer measurements. *Phys. Rev. E.* 59:3402–3407.

Crocker, J. C., M. T. Valentine, E. R. Weeks, T. Gisler, P. D. Kaplan, A. G. Yodh, and D. A. Weitz. 2000. Two-point microrheology of inhomogeneous soft materials. *Phys. Rev. Lett.* 85:888–891.

Essler, M., M. Amano, H. J. Kruse, K. Kaibuchi, P. C. Weber, and M. Aepfelbacher. 1998. Thrombin inactivates myosin light chain phosphatase via Rho and 1st target Rho kinase in human endothelial cells. *J. Biol. Chem.* 273:21867–21874.

Essler, M., M. Retzer, M. Bauer, J. M. Heemskerk, M. Aepfelbacher, and W. Siess. 1999. Mildly oxidized LDL induces contraction of human endothelial cells through activation of Rho/Rho-kinase and inhibition of myosin light chain phosphatase. *J. Biol. Chem.* 274:30361–30364.

Evans, E. A., A. Leung, and D. Zhelev. 1993. Synchrony of cell spreading and contraction force as phagocytes engulf large pathogens. *J. Cell Biol.* 122:1295–1300.

Evans, E., and R. Skalak. 1980. Mechanics and Thermodynamics of Biomembranes. CRC Press, Boca Raton, FL.

Fabry B., G. N. Maksym, J. P. Butler, M. Glogauer, D. Navajas, and J. J. Fredberg. 2001. Scaling the microrheology of living cells. *Phys. Rev. Lett.* 87:148102.

Feneberg, W. 2003. Viskoelastische mikroskopie der zellhülle von humanen endothelzellen. PhD thesis. Technische Universität München, München, Germany.

Feneberg, W., M. Westphal, and E. Sackmann. 2001. *Dictyostelium* cells' cytoplasm as active viscoplastic body. *Eur. Biophys. J.* 30:284–294.

Ferry, J. D. 1980. Viscoelastic Properties of Polymers, 3rd Ed. John Wiley & Sons, New York.

Garcia, J. G., and K. L. Schaphorst. 1995. Regulation of endothelial cell gap formation and paracellular permeability. *J. Invest. Med.* 43:117–126.

Glogauer, M., P. Arora, G. Yao, I. Sokholov, J. Ferrier, and C. A. G. McCulloch. 1997. Calcium ions and tyrosine phosphorylation interact coordinately with actin to regulate cytoprotective responses to stretching. *J. Cell Sci.* 110:11–21.

Häckl, W., U. Seifert, and E. Sackmann. 1997. Effects of fully and partially solubilized amphiphiles on bilayer bending stiffness and temperature

dependence of the effective tension of giant vesicles. *J. Phys. II* (*Fr*). 7:1141–1157.

Hall, A. 1998. Rho GTPases and the actin cytoskeleton. *Science*. 279: 509–514.

Hinner, B., M. Tempel, E. Sackmann, K. Kroy, and E. Frey. 1998. Entanglement, elasticity, and viscous relaxation of actin solutions. *Phys. Rev. Lett*. 81:2614.

Janmey, P. A. 1998. The cytoskeleton and cell signaling: component localization and mechanical coupling. *Physiol. Rev*. 78:763–781.

Jay, P. Y., P. A. Pham, S. A. Wong, and E. Elson. 1995. A mechanical function of myosin II in cell motility. *Cell Sci*. 108:387–393.

Landau, L. D., and E. M. Lifshitz. 1986. Theory of Elasticity, 3rd Ed. Pergamon Press, Oxford, UK.

Love, A. E. H. 1944. A Treatise on the Mathematical Theory of Elasticity. Dover Publications, Mineola, New York.

MacKintosh, F. C. 1998. Theoretical models of viscoelasticity of actin solutions and the actin cortex. *Biol. Bull*. 194:351–353.

Mathur, A. B., G. A. Truskey, and W. M. Reichert. 2000. Atomic force and total internal reflection fluorescence microscopy for the study of force transmission in endothelial cells. *Biophys. J*. 78:1725–1735.

Medalia, O., I. Weber, A. S. Frangakis, D. Nicastro, G. Gerisch, and W. Baumeister. 2002. Macromolecular architecture in eukaryotic cells visualized by cryoelectron tomography. *Science*. 298:1209–1213.

Merkel, R., R. Simson, D. A. Simson, M. Hohenadl, A. Boulbitch, E. Wallraff, and E. Sackmann. 2000. A micromechanical study of cell polarity and plasma membrane cell body coupling in *Dictyostelium*. *Biophys. J*. 79:707–719.

Miyamoto, S., S. K. Akiyama, and K. M. Yamada. 1995. Synergistic roles for receptor occupancy and aggregation in integrin transmembrane function. *Science*. 267:883–885.

Moolenar, W. H., O. Kranenburg, F. R. Postma, and G. C. M. Zondag. 1997. Lysophosphatidic acid: G-protein signalling and cellular responses. *Curr. Op. Cell Biol*. 9:168–173.

Moy, A. B., J. V. Engelenhoven, J. Bodmer, J. Kamath, C. Keese, I. Giaever, S. Shasby, and D. M. Shasby. 1996. Histamine and thrombin modulate endothelial focal adhesion through centripetal and centrifugal forces. *J. Clin. Invest*. 97:1020–1027.

Ohashi, T., Y. Ishii, Y. Ishikawa, T. Matsumoto, and M. Sato. 2002. Experimental and numerical analyses of local mechanical properties measured by atomic force microscopy for sheared endothelial cells. *BioMed. Mat. Eng*. 12:319–327.

Pollard, T. O., and W. C. Earnshaw. 2002. Cell Biology. W.B. Saunders, Philadelphia, PA.

Raucher, D., and M. P. Sheetz. 1999. Characteristics of a membrane reservoir buffering membrane tension. *Biophys. J*. 77:1992–2002.

Rotsch, C., and M. Radmacher. 2000. Drug-induced changes of cytoskeletal structure and mechanics in fibroblasts: an atomic force microscopy study. *Biophys. J*. 78:520–535.

Schilling, J. 2003. Entwicklung einer schnellen digitalen bildverarbeitungstechnik und interferometrischer 2λ-mikroskopietechnik: anwendung in der zell-biophysik. PhD thesis. Technische Universität München, München, Germany.

Schmidt, F. G., F. Ziemann, and E. Sackmann. 1996. Shear field mapping in actin networks by using magnetic tweezers. *Eur. Biophys. J*. 24: 348–353.

Shasby, D. M., D. R. Ries, S. S. Shasby, and M. C. Winter. 2002. Histamine stimulates phosphorylation of adherens junction proteins and alters their link to vimentin. *Am. J. Physiol. Lung Cell. Mol. Physiol.* 282:L1330–L1338.

Siess, W., K. J. Zangl, M. Essler, M. Bauer, R. Brandl, C. Corrinth, R. Bittman, G. Tigyi, and M. Aepfelbacher. 1999. Lysophosphatidic acid mediates the rapid activation of platelets and endothelial cells by mildly oxidized low density lipoprotein and accumulates in human atherosclerotic lesions. *Proc. Natl. Acad. Sci. USA*. 96:6931–6936.

Simson, R., E. Wallraff, J. Faix, J. Niewöhner, G. Gerisch, and E. Sackmann. 1998. Membrane bending modulus and adhesion energy of wild-type and mutant cells of *Dictyostelium* lacking talin or cortexillins. *Biophys. J*. 74:514–522.

Tempel, M., W. H. Goldmann, G. Isenberg, and E. Sackmann. 1995. Interaction of the 47-kDa talin fragment and the 32-kDa vinculin fragment with acidic phospholipids: a computer analysis. *Biophys. J*. 69:228–241.

Tseng, Y., T. P. Kole, and D. Wirtz. 2002. Micromechanical mapping of live cells by multiple-particle-tracking microrheology. *Biophys. J*. 83: 3162–3176.

Vonna, L., A. Wiedemann, M. Aepfelbacher, and E. Sackmann. 2003. Local force-induced conical protrusions of phagocytic cells. *J. Cell Sci*. 116:785–790.

Yarmola, E. G., T. Somasundaram, T. A. Boring, I. Spector, and M. R. Bubb. 2000. Actin-latrunculin A structure and function: differential modulation of actin-binding protein function by latrunculin A. *J. Biol. Chem*. 275:28120–28127.

Young, V. B., S. Falkow, and G. U. Schoolnik. 1992. The invasin protein of *Yersinia enterocolitica*: internalization of invasin-bearing bacteria by eukaryotic cells is associated with reorganization of the cytoskeleton. *J. Cell Biol*. 116:197–207.

Zhelev, D. V., and R. M. Hochmuth. 1995. Mechanically stimulated cytoskeleton rearrangement and cortical contraction in human neutrophils. *Biophys. J*. 68:2004–2014.

Zheng, J., P. Lamoureux, V. Santiago, T. Dennerll, R. E. Buxbaum, and S. R. Heidemann. 1991. Tensile regulation of axonal elongation and initiation. *J. Neurosci*. 11:1117–1125.

Ziemann, F., J. Rädler, and E. Sackmann. 1994. Local measurements of viscoelastic moduli of entangled actin networks using an oscillating magnetic bead microrheometer. *Biophys. J*. 66:2210–2216.